Nanoscale

Accepted Manuscript

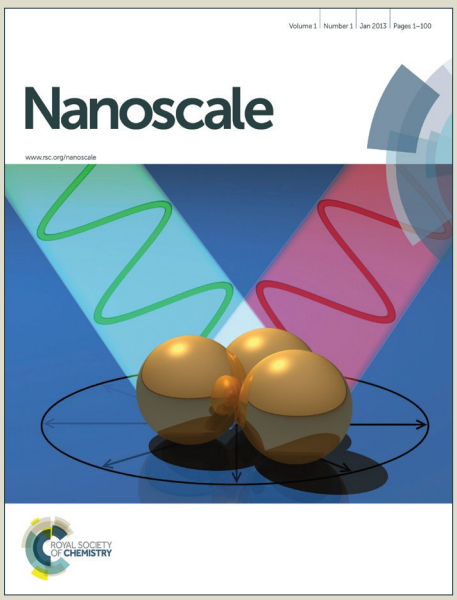

This is an *Accepted Manuscript*, which has been through the Royal Society of Chemistry peer review process and has been accepted for publication.

Accepted Manuscripts are published online shortly after acceptance, before technical editing, formatting and proof reading. Using this free service, authors can make their results available to the community, in citable form, before we publish the edited article. We will replace this *Accepted Manuscript* with the edited and formatted *Advance Article* as soon as it is available.

You can find more information about *Accepted Manuscripts* in the Information for Authors.

Please note that technical editing may introduce minor changes to the text and/or graphics, which may alter content. The journal's standard Terms & Conditions and the Ethical guidelines still apply. In no event shall the Royal Society of Chemistry be held responsible for any errors or omissions in this *Accepted Manuscript* or any consequences arising from the use of any information it contains.

ROYAL SOCIETY OF CHEMISTRY

www.rsc.org/nanoscale

Synthesis of mesoporous carbon nanoparticles with large and tunable pore sizes

Chao Liu, Meihua Yu, Yang Li, Jiansheng Li*, Jing Wang, Chengzhong Yu*, Lianjun Wang*

[*] C. Liu, Y. Li, Prof. J.S. Li, J. Wang, Prof. L.J. Wang

Jiangsu Key Laboratory of Chemical Pollution Control and Resources Reuse

School of Environmental and Biological Engineering

Nanjing University of Science and Technology

Nanjing 210094, P.R .China

E-mail: lijsh@mail.njust.edu.cn; wanglj@mail.njust.edu.cn

Dr. M.H.Yu, Prof. C.Z. Yu

Australian Institute for Bioengineering and Nanotechnology, The University of Queensland

Brisbane, QLD 4072, Australia

E-mail: c.yu@uq.edu.au

Nanoscale Accepted Manuscript

Abstract: Mesoporous carbon nanoparticles (MCNs) with large and adjustable pores have been synthesized by using poly(ethylene oxide)-*b*-polystyrene (PEO-*b*-PS) as a template and resorcinol-formaldehyde (RF) as a carbon precursor. The resultant MCNs possess small diameters (100-126 nm) and high BET surface areas (up to 646 $m^2 \cdot g^{-1}$). By using home-designed block copolymers, the pore size of MCNs can be tuned in the range of 13-32 nm. Importantly, the pore size of 32 nm is the largest among MCNs prepared by the soft-templating route. The formation mechanism and structure evolution of MCNs was studied by TEM and DLS measurements, based on which a soft-templating/sphere packing mechanism was proposed. Because of the large pores and small particle sizes, the resultant MCNs were excellent nano-carriers to deliver biomolecules into cancer cells. MCNs were further demonstrated with negligible toxicity. It is anticipated that this carbon material with large pores and small particle sizes may have excellent potential in drug/gene delivery.

Key words: Mesoporous carbon nanoparticles, large and tunable pore sizes, soft-templating, sphere packing, nano-carriers

Nanoscale Accepted Manuscript

1. Introduction

In the past two decades, nanoscience has achieved great advances in the synthesis, modification/functionalization and application of mesoporous materials. Their large specific surface area and pore volume, well-defined mesostructure, tunable pore size and open frame-work make mesoporous materials useful in many valuable applications.[1-15] Of many types of mesostructured materials that have been developed, mesoporous carbon nanoparticles (MCNs) have attracted considerable attention because of their potential applications in absorbents, drug/gene carries, fuels cells, supercapacitors and lithium batteries.[16-27] Motivated by their promising prospects, great efforts have been devoted to the preparation of MCNs. The first synthetic approach relies on hard templating with mesoporous silica spheres or colloidal crystals, which is a multiple step and complex process.[23, 28-30] The mesostructure and morphology of the replicated MCNs is limited by the parent template.[31, 32] The largest pore size of MCNs prepared by this method can reach up to 31 nm.[33] However, the size of resulting MCNs is generally in micrometer ranges, which cannot be internalized by live cells[18]. Nanoparticles with small particle size possessed advantages in cellular uptake in biomedical applications[34, 35]. Therefore, it is highly desired to fabricate small MCNs as nano-carriers for bioapplications. Recently, facile approaches such as the "silica-assisted" strategy[36] and low-concentration hydrothermal route[37] have been developed for the synthesis of MCNs. With these methods, MCNs of controllable size and morphology can be directly prepared. Nevertheless, their pore sizes are usually very small (2-5 nm), which may limit their practical applications in the encapsulation of biomolecules with large molecular weights. Hence, convenient synthesis of MCNs with both small sizes as well as large, tunable and uniform pores (larger than 10 nm) is highly desired.

Non-Pluronic amphiphilic block copolymers with high molecular weight, which have long rigid hydrophobic segments and high carbon contents, such as poly(ethylene

Nanoscale Accepted Manuscript

oxide)-*b*-polystyrene (PEO-*b*-PS), poly(isoprene)-*b*-poly(ethylene oxide) (PI-*b*-PEO), poly(ethylene-co-butylene)-*b*-poly(ethylene oxide) (KLE) and poly(ethylene oxide)-*b*-poly(methyl methacrylate) (PEO-*b*-PMMA), have been widely used as ideal templates for the synthesis of large-pore mesoporous materials.[38-47]A series of silica materials with different morphologies, including two/three-dimensional ordered mesoporous silica monoliths,[48, 49] dual-mesoporous silica monoliths,[50] and mesoporous silica spheres[51] have been fabricated. Using non-Pluronic block copolymers as templates, great success has also been achieved in the synthesis of carbon materials, including two-dimensional ordered mesoporous carbon films,[52] monoliths,[48] and hollow carbon spheres[53]. Unfortunately, high molecular weight non-Pluronic block copolymers surfactants have low water solubility, thus solvent evaporation induced self-assembly (EISA) and solvent evaporation induced aggregating assembly (EIAA) approaches are generally used to prepare mesoporous carbon materials with film or monoliths morphologies.[43] It is difficult to synthesize MCNs using non-Pluronic surfactants with both large pores and small particle sizes.

Very recently, Dai et al. reported a successful synthesis of MCNs using a non-Pluronic amphiphilic block copolymer as a soft template.[54] N-doped MCNs with a large mesopore of 16 nm and small particle size of 200 nm were obtained through the co-assembly of dopamine and a commercial diblock copolymer (PEO-*b*-PS). The resultant MCNs exhibited high electrocatalytic activity and excellent long-term stability. However, the advantage of MCNs has not been tested in bio-applications. Carbon materials have many advantages over silica materials due to their hydrophobic property and chemical inertness. [21, 55-57] Similar to silica, carbon nanoparticles are biocompatible, nontoxic, and nonimmunogenic, which allow them to be used extensively in bio-applications.[18, 58, 59] Moreover, although various formation mechanisms of silica based mesoporous materials are well-understood, such as liquid-crystal template (LCT),[60] micellar rod assembly (MRA),[61] cooperative self-assembly (CSA)[62] and

Nanoscale Accepted Manuscript

hard-sphere packing (HSP)[63]pathways, the formation mechanism of MCNs is less understood. It is of great significance to explore the formation mechanism and structure evolution of MCNs in the soft-templating strategy, which will provide insight in the design and synthesis of MCNs with new structures and properties.

Herein, we reported the synthesis of large-pore MCNs with small particle size (<150 nm) through a soft-templating/sphere packing route. By using home-designed non-Pluronic amphiphilic block copolymers (PEO-*b*-PS) as templates, the pore size of MCNs can be tuned in the range of 13-32 nm, which is the largest among MCNs prepared by soft-templating route. The structure evolution process in the formation of MCNs was clearly observed for the first time. It is demonstrated that MCNs can be utilized as nano-carriers for delivering genetic molecules into different cancer cells, showing their potential in drug/gene delivery.

2. Experimental Section

2.1 Chemicals and Materials

Monomethoxy poly (ethylene oxide) (monomethoxy PEO5000), 2-bromoisobutyrylbromide , *N,N,N',N'',N''*-pentamethyldiethylenetriamIn-e(PMDETA), and CuBr were purchased from Sigma-Aldrich. Pyridine, styrene, petroleum solution, anhydrous ethanol, formaldehyde solution (37-40 %) and resorcinol were purchased from Sinopharm Chemical Reagent Co., Ltd. Ammonia aqueous solution (25-28 %) and Tetrahydrofuran (THF) were purchased from Nanjing Chemical Reagent Co., Ltd. All chemicals were used as received without any further purification. PEO-*b*-PS copolymers, with different molecular weights (i.e., PEO_{125}-*b*-PS_{130}, PEO_{125}-*b*-PS_{178} and PEO_{125}-*b*-PS_{240}) were synthesized via sequential atomic transfer radical polymerization (ATRP) as previously reported.[48] Paraformaldehyde (PFA), twenty-one-nucleotide (oligo) DNA conjugated with cyanine dye (Cy-3), antifade fluorescent mounting medium with 4'-6-diamidino-2-phenylindole (DAPI) and 3-[4,5-dimethylthiazol-2-yl]-2,5-diphenyl tetrazolium bromide (MTT) were purchased

Nanoscale Accepted Manuscript

from Sigma-Aldrich. Fetal calf serum was purchased from Moregate Biotech, Australia. Millipore water was used in all experiments.

2.2 Synthesis of hollow carbon spheres (HCSs) and mesoporous carbon nanoparticles (MCNs)

In a typical synthesis of HCSs with a void size of 15 nm and MCNs (MCNs-1) with a pore size of 15 nm, 100 mg of PEO_{125}-*b*-PS_{178} was first dissolved in 10 mL THF. Then the above oil solution was poured into a mixture solution containing 10 mL H_2O, 10 mL ethanol and 0.1 mL ammonia. After that, resorcinol (40 mg for HCSs, 160 mg for MCNs-1) was added into the mixture oil-water-ethanol solution under mild stirring. After stirring for 30 min at 30 ^oC, formaldehyde solution (0.06 mL for HCSs, 0.2 mL for MCNs-1) was added to the reaction solution and stirred for 24 h at 30 ^oC. Then, the reaction mixture was further heated for 24 h at 100 ^oC under a static condition in a Teflon-lined autoave. The solid product was recovered by centrifugation and air-dried at 80 ^oC over night. Calcination was carried out in a tubular furnace at 800 ^oC for 3 h under N_2 flow. The heating rate was 1 ^oC min^{-1} below 450 ^oC and 5 ^oC min^{-1} above 600 ^oC. The pore sizes of MCNs were tailed by changing the diblock copolymers (PS-*b*-PEO) with different chain lengths of the PS blocks. In this work, we also used other block copolymers, such as PEO_{125}-*b*-PS_{120}, and PEO_{125}-*b*-PS_{250}. The corresponding MCNs were denoted as MCN-0, and MCN-2, respectively.

2.3 Characterization

TEM (transmission electron microscopy) analysis was conducted on a TECNAI G2 20 LaB6 electron microscope operated at 200 kV. SEM (scanning electron microscopy) analysis was conducted on FEI S4800 system. N_2 adsorption and desorption isotherms were measured using Micromeritics ASAP-2020 at liquid nitrogen temperature (-196 ^oC). The specific surface area and the pore size distribution were calculated by using the Brunauer-Emmett-Teller (BET) and nonlocal density functional theory (NLDFT) method,

Nanoscale Accepted Manuscript

respectively. The mean diameter of the samples was measured by dynamic light scattering (DLS) using a Zeta potential/particle Sizer ZetaPALS (Brookhaven, USA). Fourier transform infrared (FTIR) spectra were collected on a Nicolet Fourier spectrophotometer using KBr pellets. TGA measurements were carried out on a SDTQ600 analyzer from 25 to 800 ^{o}C under N_2 with a heating rate of 5 ^{o}C/min. The small-angle X-ray scattering (SAXS) measurements were taken on a Nanostar U SAXS system (Bruker, Germany) using Cu Kα radiation (40 kV, 35 mA).

2.4 Biological experiments

Cell culture: KHOS and HCT-116 cells were maintained in Dulbecco's Modified Eagle Medium (DMEM) supplemented with fetal calf serum (10%), L-glutamine (2%), penicillin (1%), streptomycin (1%) in 5% CO_2 at 37 °C. The medium was routinely changed every 2 days and the cells were separated by trypsinisation before reaching confluency.

Cell viability test of MCNs-1: The cytotoxicity of MCNs-1 in KHOS and HCT-116 cells was tested by the MTT method. KHOS or HCT-116 cells were seeded in a 96-well cell culture plate with a density of 5×10^3 cells/well. After incubation for 24 h, the cells were treated with different concentrations of MCNs-1 for 48 h. Afterwards, the cell viability was measured by adding MTT agent and reading the absorbance at 570 nm using a Synergy HT microplate reader. The cells incubated in the absence of particles were used as the control. All the experiments were performed in triplicates for each group. The statistical data were shown as mean±(SD).

Cellular uptake of Cy3-oligoDNA/MCNs-1: KHOS/HCT-116 cells were seeded in a 6-well plate with coverslips inside (1×10^5 cells/well) and incubated for 24 h prior to cell uptake assay. 160 μg of MCNs-1 and 2 μl of 100 μM Cy3-oligoDNA was mixed in 100 μl of phosphate buffered saline (PBS) solution and incubated at 4 °C for 4 h. After incubation, the mixture was added to the cell, and the final concentration of MCNs-1 and Cy3-oligoDNA was

Nanoscale Accepted Manuscript

80 μg/ml and 100 nM, respectively. After incubation for 4 h at 37 °C, the cells were washed twice with pre-warmed PBS, then fixed with 4% PFA in PBS solution for 20 minutes at room temperature. After washing twice with PBS again, 1 ml of absolute ethanol was added into the cell to extract water at 4 °C. The fixed cells were treated with 1% BSA in PBS solution for 30 minutes after washing with PBS twice. Alexa Fluor® 488 phalloidin staining agent was diluted and placed on the coverslip for 20 minutes at room temperature. After washing with PBS twice, the nuclei were stained with DAPI for 10 minutes. Finally, the cells were observed under a confocal microscope (LSM Zeiss 710).

3. Results and discussion

The synthesis of MCNs (e.g. MCN-1) was conducted by a self-assembly route in a mixing solvent system with PEO-*b*-PS diblock copolymer as surfactants and phenolic resol (PR) as a carbon source. Diblock copolymer PEO-*b*-PS (e.g. PEO_{125}-*b*-PS_{178}) was prepared by a simple ATRP method.[48] The successful preparation of PEO-*b*-PS was verified by ^{1}H NMR spectra (Figure S1a). The signal around 3.60 ppm is attributed to EO units. In addition, the signals around 1.20-1.63 and 6.29-7.22 ppm are ascribed to the styrene units. The Mn values of PEO-*b*-PS calculated from the ^{1}H NMR data are about 23000. As the Mn values of commercial PEO are 5000, the composition of this block copolymer can be approximately formulated as PEO_{125}-*b*-PS_{178}. Gel permeation chromatography (GPC) showed a polydispersity index (PDI) of 1.18 (Figure S1b), indicating a narrow molecular-weight distribution.

The SEM images of as-synthesized PR/PEO_{125}-*b*-PS_{178} composites nanoparticles before carbonization are present in Figure S2a, b. The PR/PEO_{125}-*b*-PS_{178} composites nanoparticles have a spherical morphology with an average size of 160 nm. At a higher magnification, it can be seen that each sphere is composed of even smaller spheres with an average diameter of 33 nm. From the TEM images of PR/PEO-*b*-PS composites nanoparticles (Figure S2c, d), it is

Nanoscale Accepted Manuscript

also revealed that the large particles are generated by the gathering of smaller particles, which is consistent with SEM results. After heat treatment at 700 ^{o}C in N_2 atmosphere, the PR/PEO_{125}-*b*-PS_{178} composites nanoparticles were carbonized to MCNs, denoted as MCNs-1. The average size of MCNs-1 is decreased to 126 nm compared with PR/PEO_{125}-*b*-PS_{178} composites nanoparticles (Figure 1a), due to the shrinkage of carbon precursors during the carbonization process. It can be clearly observed that uniformly sized mesopores are well distributed on the particle surface (Figure 1b). The mesostructure and interior construction of obtained MCNs-1 were further investigated by TEM. Extensive mesopores can be found distributing throughout the whole particles (MCNs-1) after carbonization (Figure 1c), in correspondence with the SEM measurements. The diameters of large mesopores measured from Figure 1d are about 17.5 nm in average. From the rough surface of PR/PEO_{125}-*b*-PS_{178} composites nanoparticles and mesoporous structure of MCNs-1, it is reasonable to deduce that the mesopores are generated from PEO_{125}-*b*-PS_{178} templates.

To support the above conclusion, PR polymers were prepared without using PEO_{125}-*b*-PS_{178} surfactant. Figure S3, ESI shows the SEM and TEM images for PR polymers. Unlike PR/PEO_{125}-*b*-PS_{178} composites nanoparticles, the PR polymers show typical spherical morphology and very smooth surface, similar to the results of stöber-carbon system.[64] Subsequently, the obtained PR spheres were also thermally converted to carbon spheres (CSs). The resultant CSs keep the spherical morphology and smooth surface, with no mesopores throughout the particles. The results further prove the pore-forming role of PEO_{125}-*b*-PS_{178}.

The N_2 sorption isotherms of MCNs-1 and CSs are shown in Figure 2a and S4, respectively. MCNs-1 exhibits type IV isotherms with a hysteresis loop in the high relative pressure range of 0.85-0.95, indicating the presence of uniform and large pores in MCNs-1. The diameter of the mesopores was calculated to be ~18.0 nm from the adsorption branch by the nonlocal density functional theory (NLDFT) model (inset of Figure 2a), which is

Nanoscale Accepted Manuscript

consistent with the TEM measurements. Nevertheless, without the templates, CSs show type I isotherms, implying the microporous structure of CSs. In addition, the specific surface area and total pore volume of MCNs-1 are 646 $m^2 \cdot g^{-1}$ and 0.63 $cm^3 \cdot g^{-1}$, respectively. The specific surface area and total pore volume of CSs are 545 $m^2 \cdot g^{-1}$ and 0.27 $cm^3 \cdot g^{-1}$. The small angle X-ray scattering (SAXS) pattern of MCNs-1 was shown in Figure 2b, from which a closest d-spacing between two adjacent pores of 23.9 nm was calculated. This result was in accordance with the measurement of TEM image.

The TGA curve (Figure S5) of as-made MCNs-1 shows several obvious weight-loss stages. The weight loss about 10% below 300 ^oC can be assigned to the removal of water both physically adsorbed and generated from further condensation. Large weight loss between 300 ^oC and 700 ^oC is about 55%, which can be ascribed to the decomposition of PEO_{125}-*b*-PS_{178} and pyrolysis of PR framework, suggesting that the template can be removed at 430 ^oC. After carbonization at 800 ^oC, the yields for MCNs-1 are calculated to be 35% based on carbon content. The FT-IR spectrums of PR/PEO_{125}-*b*-PS_{178} composites particles (a) and MCNs-1 (b) were shown in Figure S6. In the curve (a), the strong and broad band at 3400 cm^{-1} is associated with the phenolic –OH groups, and the bands at 1100 cm^{-1} and 2800 cm^{-1} are assigned to PEO block and PS block, respectively.[46, 48] The disappearance of characteristic bands at 1100 and 2800 cm^{-1} in curve (b) suggest the decomposition of PEO-*b*-PS and pyrolysis of RF framework. Meanwhile, no adsorption was observed in curve (b), suggesting a carbon framework feature after carbonization at 700 ^oC. In addition, the nature of carbon species on the surface of MCNs-1 was further investigated by XPS. Figure S7a is the XPS survey spectra of MCNs-1, which shows the peaks of C1s and O1s, indicating the indicating the existence of C and O in the carbon framework. The high-resolution XPS spectra of C1s (Figure S7b) can be curve-fitted into three-type peaks arising from C=C (284.7 ± 0.1 eV), C-O (286.5 ± 0.1 eV) and O-C=O (289.0 ± 0.1 eV), which is similar to the conventional

Nanoscale Accepted Manuscript

mesoporous carbon materials[65] (Figure S7c, d). The above mentioned characterizations have confirmed that MCNs-1 with large mesopores (ca. 18.0 nm) and small dimensions (ca. 126 nm) have been successfully prepared

To gain insights into the formation mechanism, TEM was employed to monitor the structure evolution as a function of time (Figure 3). In the experimental process, PEO_{125}-*b*-PS_{178} was firstly mixed in THF solution, in which it was completely dissolved. After adding water and ethanol, the micellization process occurred, in which the Tyndall effect was clearly observed (Figure 4b). The TEM image of 0 h shows the presence of the PEO-*b*-PS micelles with a diameter of about 27 nm (Figure 3a). After addition of carbon precursors, the PR resins were slowly generated with the polymerization of resorcinol and formaldehyde. Due to the hydrogen bonding between the PR resin and the -OH groups in PEO block,[37] PR particles deposit on the PEO chains of PEO_{125}-*b*-PS_{178} micelle and form PR/PEO_{125}-*b*-PS_{178} composite micelles. The size of composite micelles was slightly expanded to 32 nm, as measured from the TEM image at 5 h (Figure 3b). Meanwhile, the reaction solution transformed from light blue to light yellow. The Tyndall effect was still clearly observed (Figure S4c, d), indicating the generation of PR/PEO_{125}-*b*-PS_{178} composite micelles. When the reaction time was prolonged to 6 h, some larger particles with a diameter of about 65 nm were observed (Figure 3c). After further reaction for 1h, the composite nanoparticles had a larger size of ~122 nm, with clearly decreased amount of PR/PEO_{125}-*b*-PS_{178} composite micelles (Figure 3d). With the reaction time increased to 8 h, the PR/PEO_{125}-*b*-PS_{178} composite nanoparticles with a diameter of ~145 nm were observed (Figure 3e). After constantly stirring for 12 h, barely PR/PEO_{125}-*b*-PS_{178} composite micelles were found, indicating the completion of reaction from composite micelles packing into composite nanopartciels. The PR/PEO-*b*-PS composite nanoparticles finally formed had a diameter of 166 nm (Figure 3f), in accordance with the SEM and TEM results in Figure S1. It can be

Nanoscale Accepted Manuscript

concluded that spherical composite micelles are formed through soft templating between PR and PEO_{125}-*b*-PS_{178}, which further pack into PR/PEO_{125}-*b*-PS_{178} composite nanoparticle, similar to the HSP pathway in mesoporous silica systems.[63]

DLS was also used to monitor the evolution of particles formed during the assembly process (Figure 4a). The results show that the origin particle size of PEO-*b*-PS micelle was about 29 nm. After 5 h, two new peaks at 5 nm and 35 nm were observed, which are attributed to the PR particles and PR/PEO_{125}-*b*-PS_{178} composite micelles. After 6 h, another new peak was appeared at 65 nm due to the aggregation of PR/PEO_{125}-*b*-PS_{178} composite micelles. The disappearance of the peak at 5 nm suggests that most of the PR particles assemble with PEO_{125}-*b*-PS_{178} micelle into PR/PEO_{125}-*b*-PS_{178} composite micelles. After 7 h, the peak of aggregates shifts to the larger diameter of about 123 nm. Meanwhile, the peak at 35 nm is apparently weakened, indicating the further aggregation of PR/PEO_{125}-*b*-PS_{178} composite micelles. After 8 h, the composite particles grow to the final form, with size of around 145 nm following the continuously weakened peak density at 35 nm. After 12 h, single well-resolved peak at 170 nm is detected. Meanwhile, the peak of PR/PEO-*b*-PS composite micelle is disappeared, implying the completion of reaction. The results of DLS are absolutely consistent with the TEM measurements in Figure 3.

In order to acquire more information on the formation mechanism, a synthesis with a relatively low PR concentration was conducted keep the other synthesis parameters unchanged. After carbonization in N_2, hollow carbon spheres (HCSs) were obtained (Figure 5a, b). The diameter of the hollow spheres is measured to 32 nm, with a mean shell thickness of 7 nm and void size of 18 nm. The N_2 sorption isotherm and the pore size distribution cure of HCSs are present in Figure 5c. It can be seen that HCSs exhibits type IV isotherms with a hysteresis loop in the high relative pressure range of 0.85-0.95, similar to the isotherms of MCNs, indicating the presence of uniform and large mesopores. The pore size distribution of

Nanoscale Accepted Manuscript

HCSs is centered at 17.5 nm (inset in Figure 5c), consistent with the void size of HCSs and the mesopores diameter of MCNs measured from TEM. The specific surface area and total pore volume of HCSs are about 673 $m^2 \cdot g^{-1}$ and 0.67 $cm^3 \cdot g^{-1}$, respectively. The as-synthesized HCSs also show similar well-resolved SAXS pattern with MCNs at q around 0.027 A^{-1}, from which a closest d-spacing between two adjacent pores of 23.3 nm was calculated (Figure 5d). As reported previously [63, 66, 67], the SAXS peak may be attributed to the short-range periodicity of closely packed nanospheres.

Based on the results mentioned above, we propose that the MCNs in our synthesis form by a soft-templating/sphere packing pathway, as described in Scheme 1. The PEO-*b*-PS micelles are pre-formed in water, ethanol, THF and block polymer PEO-*b*-PS mixed solution. With the addition of carbon precursors (resorcinol and formaldehyde), the assembly between PR resin and PEO-*b*-PS micelle is initiated. The PR/PEO-*b*-PS composite micelles are generated in the solution. As the reaction proceed, the spherical PR/PEO-*b*-PS composite micelles with diameter of 35 nm are spontaneously packed to PR/PEO-*b*-PS composite nanoparticles with size of 160 nm. After carbonization in N_2 at 700 ^oC, MCNs with mesopores (ca.18 nm) can be obtained. In our approach, the PEO-*b*-PS micelles act as a sacrificial pore-forming agent during carbonization. The mesopore sizes observed on the surface of the NMCS are slightly smaller than the micelle sizes observed on the original PR/PEO-*b*-PS composite micelles, due to thermal shrinkage of the pore walls. The lower concentration of carbon precursor results in the formation of composite micelles, but the further packing to composite nanoparticles is not favored. Consequently, individual hollow carbon spheres with a diameter of 32 nm and a void size around 18 nm were formed. Notably, these small-sized HCSs, which are considered as building block for the formation of MCNs, are not reported in previous studies.

The influence of temperature and ethanol on the structure of MCNs was also investigated.

Nanoscale Accepted Manuscript

When the reaction temperature was decreased to 20 ^{o}C, MCNs with smaller particle size of 100 nm was obtained (Figure S8a). While increasing temperature to 40 ^{o}C, MCNs with a mean particle size of ~170 nm was observed in the TEM image (Figure S8a). It can be concluded that a relatively higher reaction temperature leads to MCNs with larger particle sizes, which may be ascribed to the acceleration of temperature to the sphere packing process. When adjusting the amount of ethanol in the range of 5-15 mL, no obvious change on the structure and particle size of MCNs was observed (Figure S8c, d). These result further confirmed the soft-templating/sphere packing mechanism.

To demonstrate the versatility of our approach, block copolymers with the same composition but different polymerization degree of PS, namely, PEO_{125}-*b*-PS_{120}, and PEO_{125}-*b*-PS_{250}, can also be prepared and used as templates to synthesize MCNs. Mesoporous carbon nanopartiles with diameters of ～100 nm (denote MCNs-0 and MCNs-2) were obtained. The TEM and SEM images of MCNs-0 and MCNs-2 demonstrate the uniform distribution of the large mesopores with diameters of about 12.5 and 31.2 nm (Figure 6). N_2 adsorption isotherms of MCNs-0 and MCNs-2 shows type IV curves with a large hysteresis loop, suggesting a uniform mesopore (Figure S9 a, b). The special surface areas, total pore volumes, and average pore sizes of MCNs-0 and MCNs-2 are summarized in Table 1. The as-synthesized MCNs-0 and MCNs-2 show primary mesopores sizes centered at 13.0 and 32.0 nm, respectively (Figure S9 c, d). These values are almost the same as those observed by SEM and TEM. The TEM images and DLS profiles of PEO-b-PS micelles, including PEO_{125}-*b*-PS_{120} micelle, PEO_{125}-*b*-PS_{178} micelle and PEO_{125}-*b*-PS_{250} micelle, were present in Figure S10. The size of micelles are 23.0, 29.0, 41.8 nm, respectively. Clearly, with increasing PS block weight in PEO-*b*-PS, the sizes of micelles are expanding. In addition, the pore sizes of MCN-0, MCN-1 and MCN-2 are also increased with micelle sizes (Figure S11). These results show that our proposed mechanism is general. In addition, the pore size of MCNs can

Nanoscale Accepted Manuscript

be adjusted by tuning the hydrophobic moiety of block copolymers. It is noted that the resultant pore size of 32.0 nm (MCN-2) is larger than any previously reported MCNs synthesized by soft templating, which may be attributed to the longer PS chains of the home-designed PEO-*b*-PS block copolymer.[37, 54]

To demonstrate the potential applications of MCNs as nano-carriers to deliver biomolecules into cancer cells, the cyanine dye-labelled oligoDNA (Cy3-oligoDNA) was chosen as a model. As shown in Figure 7, no Cy3 signals (red fluorescence) are observed in human colon cancer cells (HCT-116) without any treatment (first row) or treated with Cy3-oligoDNA alone (second row), indicating that the cells cannot take up negatively charged molecules. In contrast, strong Cy3 signals localizes within the cell borders when MCNs-1 is utilized to deliver Cy3-oligoDNA. A similar observation can also be found in osteosarcoma cells (KHOS) (Figure S12). These results suggest that MCNs-1without any surface modification can efficiently deliver the biomolecules into different cancer cells. The biocompatibility of MCNs-1 was also evaluated, which shows negligible toxicity in both HCT-116 and KHOS cells at concentrations from 10-80 μg/ml (Figure S13). Considering their large pores, small particle sizes and direct interaction with biomolecules, this carbon material may have excellent potential in drug/gene/protein delivery.

4. Conclusion

In summary, mesoporous carbon nanoparticles (MCNs) with high BET surface area (up to 646 $m^2 \cdot g^{-1}$), tunable large pore size (13-32 nm), and small diameter (100-126 nm) have been successfully designed and fabricated by a soft-templating/ sphere packing route by using non-Pluronic amphiphilic block copolymers as templates and phenolic resol (PR) as a carbon source. Block copolymers and the phenolic resol oligomers spontaneously self-assemble into spherical micelles, subsequently, the composite micelles then pack into composite nanoparticles. By tuning the molecular weight of block copolymers, the pore size of resultant

Nanoscale Accepted Manuscript

MCNs can be adjusted. Because of the large pores and small particle sizes, MCNs are excellent nano-carriers to deliver biomolecules into cancer cells. It is anticipated that MCNs may have promising applications in drug/gene/protein delivery.

Acknowledgments

This work was financially supported by the National Natural Science Foundation of China (Grant No. 51478224) and the priority academic program development of Jiangsu higher education institutions. We acknowledge the technical support from the Australian National Fabrication Facility (ANFF), The University of Queensland, Australia.

References

1. Hartmann, M, *Chem.Mater.* 2005**,** 17, 4577.
2. Meng, Y.; Gu, D.; Zhang, F. Q.; Shi, Y. F.; Yang, H. F.; Li, Z.; Yu, C. Z.; Tu, B.; Zhao, D. Y, *Angew. Chem. Int. Ed.* 2005**,** 44, 7053.
3. Ryoo, R.; Joo, S. H.; Kruk, M.; Jaroniec, M, *Adv. Mater.* 2001**,** 13, 677.
4. Scott, B. J.; Wirnsberger, G.; Stucky, G. D, *Chem. Mater.* 2001**,** 13, 3140.
5. Shi, J. L, *Chem. Rev.* 2013**,** 113, 2139.
6. Vallet-Regi, M.; Balas, F.; Arcos, D, *Angew. Chem. In. Ed.* 2007**,** 46, 7548.
7. Zhang, F. Q.; Meng, Y.; Gu, D.; Yan, Y.; Yu, C. Z.; Tu, B.; Zhao, D. Y, *J. Am. Chem. Soc.* 2005**,** 127, 13508.
8. Yu, C. Z.; Tian, B. Z.; Fan, J.; Stucky, G. D.; Zhao, D. Y, *J. Am. Chem. Soc.* 2002**,** 124, 4556.
9. Yu, C. Z.; Fan, J.; Tian, B. Z.; Zhao, D. Y.; Stucky, G. D, *Adv. Mater.* 2002**,** 14, 1742.
10. Popat, A.; Jambhrunkar, S.; Zhang, J.; Yang, J.; Zhang, H. W.; Meka, A.; Yu, C. Z, *Chem. Comm.* 2014**,** 50, 5547.
11. Jambhrunkar, S.; Yu, M.; Yang, J.; Zhang, J.; Shrotri, A.; Endo-Munoz, L.; Moreau, J.; Lu, G.; Yu, C, *J. Am. Chem. Soc.* 2013**,** 135, 8444.
12. Yu, C. Z.; Fan, J.; Tian, B. Z.; Zhao, D. Y, *Chem. Mater.* 2004**,** 16, 889.
13. Li, J. S.; Miao, X. Y.; Hao, Y. X.; Zhao, J. Y.; Sun, X. Y.; Wang, L. J, *J. Colloid. Interf. Sci.* 2008**,** 318, 309.
14. Liu, C.; Li, J. S.; Qi, J. W.; Wang, J.; Luo, R.; Shen, J. Y.; Sun, X. Y.; Han, W. Q.; Wang, L. J, *Acs Appl. Mater. Interf.* 2014**,** 6, 13167.
15. Li, J. S.; Gu, J.; Li, H. J.; Liang, Y.; Hao, Y. X.; Sun, X. Y.; Wang, L. J, *Microporous Mesoporous Mater.* 2010**,** 128, 144.
16. Wu, Z. X.; Wu, W. D.; Liu, W. J.; Selomulya, C.; Chen, X. D.; Zhao, D. Y, *Angew. Chem. In. Ed.* 2013**,** 52, 13764.
17. Wang, Z. Y.; Li, F.; Stein, A, *Nano Lett.* 2007**,** 7, (10), 3223-3226.
18. Kim, T. W.; Chung, P. W.; Slowing, II; Tsunoda, M.; Yeung, E. S.; Lin, V. S. Y, *Nano Lett.* 2008**,** 8, 3724.
19. Sun, Z. K.; Liu, Y.; Li, B.; Wei, J.; Wang, M. H.; Yue, Q.; Deng, Y. H.; Kaliaguine, S.; Zhao, D. Y, *Acs Nano* 2013**,** 7, 8706.
20. Lei, Z. B.; Christov, N.; Zhang, L. L.; Zhao, X. S, *J. Mater. Chem.* 2011**,** 21, 2274.
21. Liu, H. J.; Cui, W. J.; Jin, L. H.; Wang, C. X.; Xia, Y. Y. *J. Mater. Chem.* 2009**,** 19, 3661.

Nanoscale Accepted Manuscript

22. Yan, X.; Song, H. H.; Chen, X. H, *J. Mater. Chem.* 2009**,** 19, 4491.
23. Fuertes, A. B, *J. Mater. Chem.* 2003**,** 13, 3085.
24. Joo, S. H.; Lee, H. I.; You, D. J.; Kwon, K.; Kim, J. H.; Choi, Y. S.; Kang, M.; Kim, J. M.; Pak, C.; Chang, H.; Seung, D, *Carbon* 2008**,** 46, 2034.
25. Fan, Y.; Yang, X.; Zhu, B.; Liu, P. F.; Lu, H. T, *J. Power Sources* 2014**,** 268, 584.
26. Liu, W. J.; Liu, Y. X.; Yan, X. Y.; Yong, G. P.; Xu, Y. P.; Liu, S. M, *J. Mater. Chem. A.* 2014**,** 2, 9600.
27. Chen, Y.; Song, B. H.; Li, M.; Lu, L.; Xue, J. M, *Adv. Funct. Mate.* 2014**,** 24, 319.
28. Yan, Y.; Zhang, F. Q.; Meng, Y.; Tu, B.; Zhao, D. Y, *Chem. Comm.* 2007, 2867.
29. Hampsey, J. E.; Hu, Q. Y.; Rice, L.; Pang, J. B.; Wu, Z. W.; Lu, Y. F, *Chem. Comm.* 2005, 3606.
30. Xia, Y. D.; Mokaya, R, *Adv. Mater.* 2004**,** 16, 886.
31. Wan, Y.; Yang, H. F.; Zhao, D. Y, *Acc. Chem. Res.* 2006**,** 39, 423.
32. Ma, X. M.; Gan, L. H.; Liu, M. X.; Tripathi, P. K.; Zhao, Y. H.; Xu, Z. J.; Zhu, D. Z.; Chen, L. W, *J. Mater. Chem. A.* 2014**,** 2, 8407.
33. Li, W. R.; Chen, D. H.; Li, Z.; Shi, Y. F.; Wan, Y.; Wang, G.; Jiang, Z. Y.; Zhao, D. Y, *Carbon*. 2007, 45, 1757.
34. Lu, F.; Wu, S. H.; Hung, Y.; Mou C. Y. Small. 2009, 12, 1408
35. Yu, M.H.; Karmakar, S.; Yang, Jie.; Zhang, H. W.; Yang, Y. N.; Thornb, P.; Yu, C. Z. *Chem. Comm.* 2014, 50, 1527.
36. Qiao, Z. A.; Guo, B. K.; Binder, A. J.; Chen, J. H.; Veith, G. M.; Dai, S, *Nano Lett.* 2013**,** 13, 207.
37. Fang, Y.; Gu, D.; Zou, Y.; Wu, Z. X.; Li, F. Y.; Che, R. C.; Deng, Y. H.; Tu, B.; Zhao, D. Y, *Angew. Chem. In. Ed.* 2010**,** 49, 7987.
38. Li, Y. H.; Luo, W.; Qin, N.; Dong, J. P.; Wei, J.; Li, W.; Feng, S. S.; Chen, J. C.; Xu, J. Q.; Elzatahry, A. A.; Es-Saheb, M. H.; Deng, Y. H.; Zhao, D. Y, *Angew. Chem. In. Ed.* 2014**,** 53, 9035.
39. Li, Y. H.; Wei, J.; Luo, W.; Wang, C.; Li, W.; Feng, S. S.; Yue, Q.; Wang, M. H.; Elzatahry, A. A.; Deng, Y. H.; Zhao, D. Y, *Chem. Mater.* 2014**,** 26, 2438.
40. Li, W.; Yue, Q.; Deng, Y. H.; Zhao, D. Y, *Adv. Mater.* 2013**,** 25, 5129.
41. Wang, C.; Wei, J.; Yue, Q.; Luo, W.; Li, Y. H.; Wang, M. H.; Deng, Y. H.; Zhao, D. Y, *Angew. Chem. In. Ed.* 2013**,** 52, 11603.
42. Wei, J.; Li, Y. H.; Wang, M. H.; Yue, Q.; Sun, Z. K.; Wang, C.; Zhao, Y. J.; Deng, Y. H.; Zhao, D. Y, *J. Mater. Chem.A.* 2013**,** 1, 8819.
43. Deng, Y. H.; Wei, J.; Sun, Z. K.; Zhao, D. Y, *Chem. Soc. Rev.* 2013**,** 42, 4054.
44. Zhang, J. Y.; Deng, Y. H.; Gu, D.; Wang, S. T.; She, L.; Che, R. C.; Wang, Z. S.; Tu, B.; Xie, S. H.; Zhao, D. Y, *Adv. Energy Mater.* 2011**,** 1, 241.
45. Deng, Y. H.; Cai, Y.; Sun, Z. K.; Gu, D.; Wei, J.; Li, W.; Guo, X. H.; Yang, J. P.; Zhao, D. Y, *Adv. Funct. Mater.* 2010**,** 20, 3658.
46. Deng, Y. H.; Liu, J.; Liu, C.; Gu, D.; Sun, Z. K.; Wei, J.; Zhang, J. Y.; Zhang, L. J.; Tu, B.; Zhao, D. Y, *Chem. Mater.* 2008**,** 20, 7281.
47. Deng, Y.; Liu, C.; Gu, D.; Yu, T.; Tu, B.; Zhao, D, *J. Mater. Chem.* 2008**,** 18, 91.
48. Deng, Y. H.; Yu, T.; Wan, Y.; Shi, Y. F.; Meng, Y.; Gu, D.; Zhang, L. J.; Huang, Y.; Liu, C.; Wu, X. J.; Zhao, D. Y, *J. Am. Chem. Soc.* 2007**,** 129, 1690.
49. Wei, J.; Wang, H.; Deng, Y. H.; Sun, Z. K.; Shi, L.; Tu, B.; Luqman, M.; Zhao, D. Y, *J. Am. Chem. Soc.* 2011**,** 133, 20369.
50. Wei, J.; Yue, Q.; Sun, Z. K.; Deng, Y. H.; Zhao, D. Y, *Angew. Chem. In. Ed.* 2012**,** 51, 6149.
51. Niu, D. C.; Liu, Z. J.; Li, Y. S.; Luo, X. F.; Zhang, J. Y.; Gong, J. P.; Shi, J. L, *Adv. Mater.* 2014**,** 26, 4947.

Nanoscale Accepted Manuscript

52. Liang, C. D.; Hong, K. L.; Guiochon, G. A.; Mays, J. W.; Dai, S, *Angew. Chem. In. Ed.* 2004**,** 43, 5785.
53. Li, Z. H.; Wu, D. C.; Huang, X.; Ma, J. H.; Liu, H.; Liang, Y. R.; Fu, R. W.; Matyjaszewski, K, *Energy Environ. Sci.* 2014**,** 7, 3006.
54. Tang, J.; Liu, J.; Li, C. L.; Li, Y. Q.; Tade, M. O.; Dai, S.; Yamauchi, Y, *Angew. Chem. In. Ed.* 2015**,** 54, 588.
55. Li, W. R.; Chen, D. H.; Li, Z.; Shi, Y. F.; Wan, Y.; Huang, J. J.; Yang, J. J.; Zhao, D. Y.; Jiang, Z. Y, *Electrochem. Comm.* 2007**,** 9, 569.
56. Chang, H.; Joo, S. H.; Pak, C, *J. Mater. Chem.* 2007**,** 17, 3078.
57. Yuan, Z. Y.; Su, B. L, *J. Mater. Chem.* 2006**,** 16, 663.
58. Guo, Y. G.; Hu, Y. S.; Maier, J, *Chem. Comm.* 2006, 2783.
59. Chen, Y.; Xu, P. F.; Wu, M. Y.; Meng, Q. S.; Chen, H. R.; Shu, Z.; Wang, J.; Zhang, L. X.; Li, Y. P.; Shi, J. L, *Adv. Mater.* 2014**,** 26, 4294.
60. Kersge, C. T.; Leonowicz, M. E.; Roth, W. J.; Vartuli, J. C.; Beck, J. S, *Nature*. 1992, 359, 710.
61. Chen, C. Y.; Burkett, S. L.; Li, H. X.; Davis, M. E, *Microporous Mater*. 1993, 2, 27.
62. Morrier, A.; Schuth, F.; Huo, Q.; Kumar, D.; Margolese, D.; Maxwell, R. S.; Stucky, G. D.; Krishnamurty, M.; Petroff, P.; Firouzi, A.; Janicke, M.; Chmelka, B. F, *Science*, 1993, 261, 1299
63. Tang, J. W.; Zhou, X. F.; Zhao, D. Y.; Lu, G. Q.; Zou, J.; Yu, C. Z, *J. Am. Chem. Soc.* 2007**,** 129, 9044.
64. Liu, J.; Qiao, S. Z.; Liu, H.; Chen, J.; Orpe, A.; Zhao, D. Y.; Lu, G. Q, *Angew. Chem. In. Ed.* 2011**,** 50, 5947.
65. Meng, Y.; Gu, D.; Zhang, F. Q.; Shi, Y. F.; Yang, H. F.; Li, Z.; Yu, C. Z.; Tu, B.; Zhao, D. Y, *Angew. Chem. In. Ed.* 2005, 44, 7053.
66. Yokoi, T.; Sakamoto, Y.; Terasaki, O.; Kubota, Y.; Okubo, T.; Tatsumi, T. *J. Am. Chem. Soc*. 2006, 128, 13664.
67. Liu, J.; Yang, Q. H.; Zhang, L.; Yang, H. Q.; Gao, J. S.; Li, C. *Chem. Mater.* 2008, 20, 4268.

Nanoscale Accepted Manuscript

Figure captions

Figure 1. SEM images (a, b) and TEM images (c, d) of mesoporous carbon nanoparticles (MCNs-1).

Figure 2. (a) nitrogen adsorption-desorption isotherm and NLDFT pore diameter distribution curve from adsorption branch (inset of a) of MCNs-1, (b) SAXS pattern of MCNs-1.

Figure 3. TEM images of samples obtained from the solution PEO125-b-PS178/THF/H_2O/ NH_3/ resorcinol/formaldehyde after reacting for: (a) 0h, (b) 5h, (c) 6h, (d) 7h, (e) 8h, (f) 12h.

Figure 4. (a) Dynamic light scattering (DLS) profiles obtained from the solution PEO_{125}-*b*-PS_{178}/THF/H_2O/NH_3/resorcinol/formaldehyde after reacting for: 0h, 5h, 6h, 7h, 8h, 12h, Photograph of (b) PEO_{125}-*b*-PS_{178} micelles, (c, d) the solution PEO_{125}-*b*-PS_{178}/THF/H_2O/NH_3/resorcinol/formaldehyde after reacting for 5h.

Figure 5. (a, b) TEM images of single hollow carbon spheres (HCSs), (c) nitrogen adsorption-desorption isotherm and NLDFT pore diameter distribution curve from adsorption branch (inset of c) of HCSs, (d) SAXS pattern of HCSs.

Scheme 1. Schematic illustration of the formation process of the mesoporous carbon nanoparticles (MCNs) by a soft-templating/sphere packing pathway.

Figure 6. (a, b) SEM image and TEM image of MCN-0, (c, d) SEM image and TEM image of MCN-2.

Figure 7. Confocal microscopy images of HCT-116 cells only without any treatment (first row), with the treatment of free Cy3-Oligo DNA (100nM) (second row), the complex of MCNs-1 (80 ug/ml) and Cy3-Oligo DNA (100nM) (third row). The cytosols and nuclei in cells were stained by Alexa Fluor® 488 phalloidin(green) and DAPI (blue), respectively.

Nanoscale Accepted Manuscript

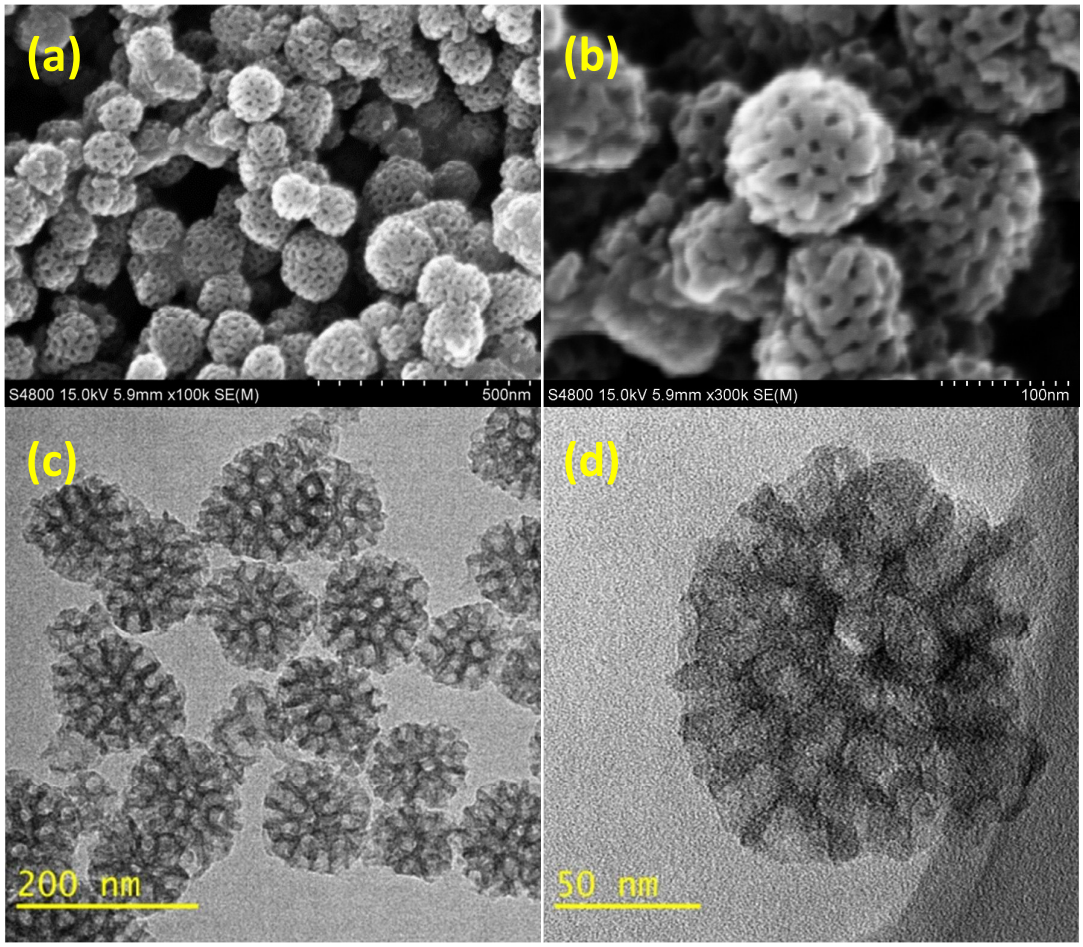

Figure 1. SEM images (a, b) and TEM images (c, d) of mesoporous carbon nanoparticles (MCNs-1).

Nanoscale Accepted Manuscript

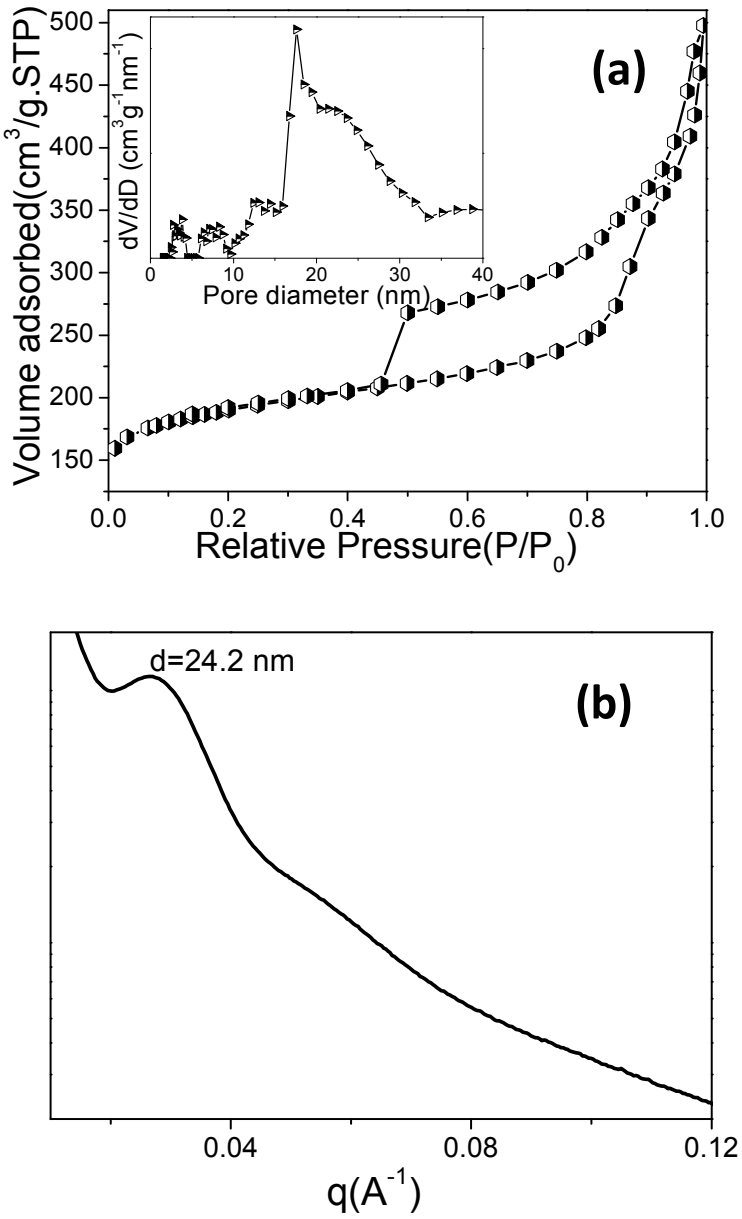

Figure 2. (a) nitrogen adsorption-desorption isotherm and NLDFT pore diameter distribution curve from adsorption branch (inset of a) of MCNs-1, (b) SAXS pattern of MCNs-1.

Nanoscale Accepted Manuscript

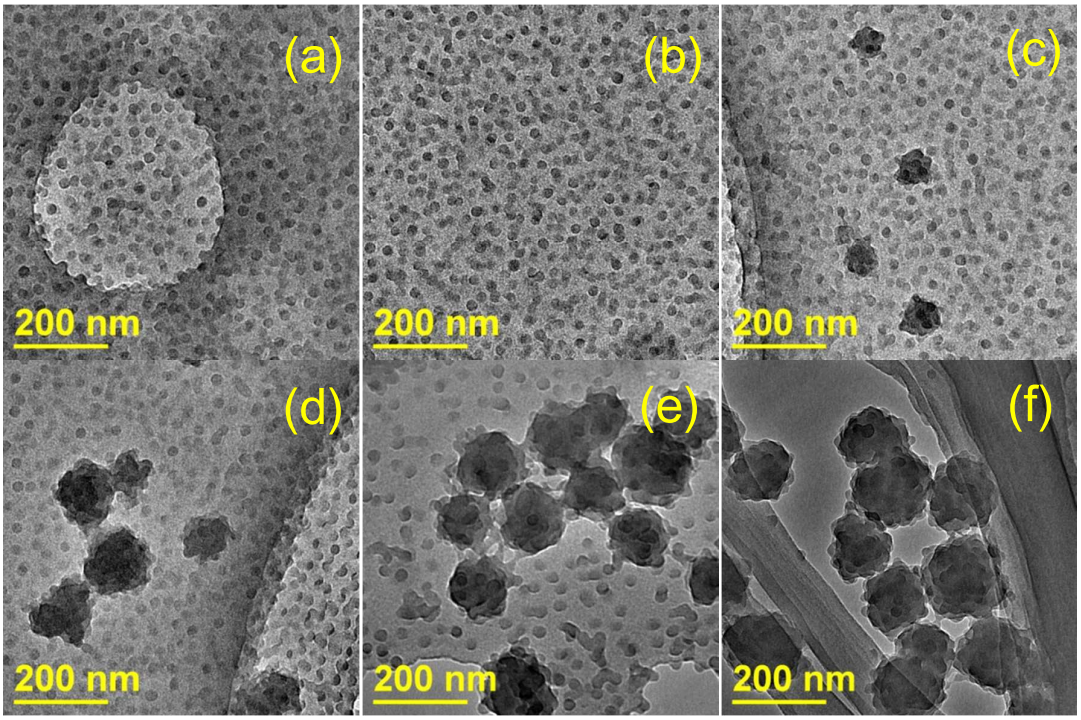

Figure 3. TEM images of samples obtained from the solution PEO_{125}-*b*-PS_{178}/THF/ H_2O/NH_3/ resorcinol/formaldehyde after reacting for: (a) 0h, (b) 5h, (c) 6h, (d) 7h, (e) 8h, (f) 12h.

Nanoscale Accepted Manuscript

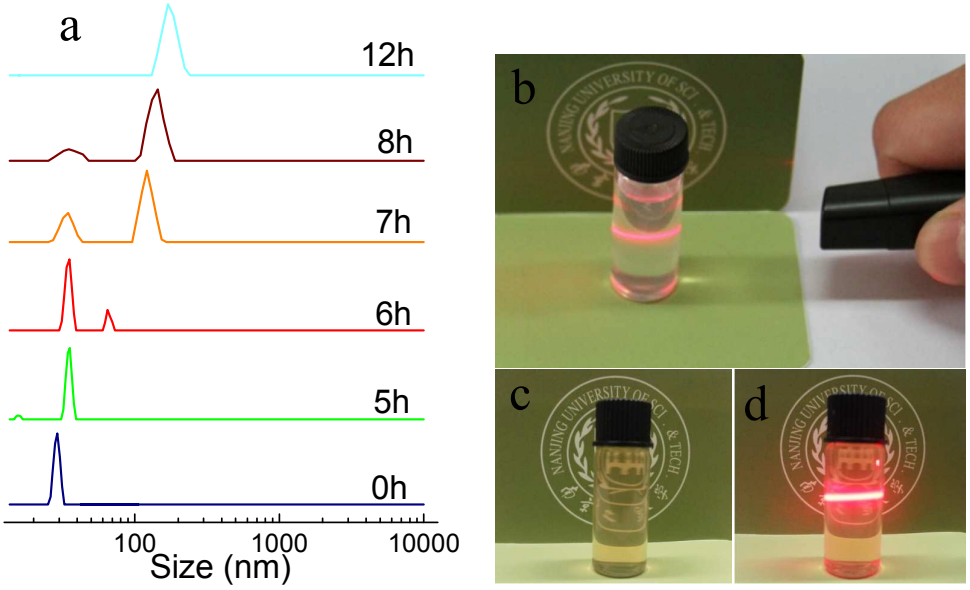

Figure 4. (a) Dynamic light scattering (DLS) profiles obtained from the solution PEO_{125}-*b*-PS_{178}/THF/H_2O/NH_3/resorcinol/formaldehyde after reacting for: 0h, 5h, 6h, 7h, 8h, 12h, Photograph of (b) PEO_{125}-*b*-PS_{178} micelles, (c, d) the solution PEO_{125}-*b*-PS_{178}/THF/H_2O/NH_3/resorcinol/formaldehyde after reacting for 5h.

Nanoscale Accepted Manuscript

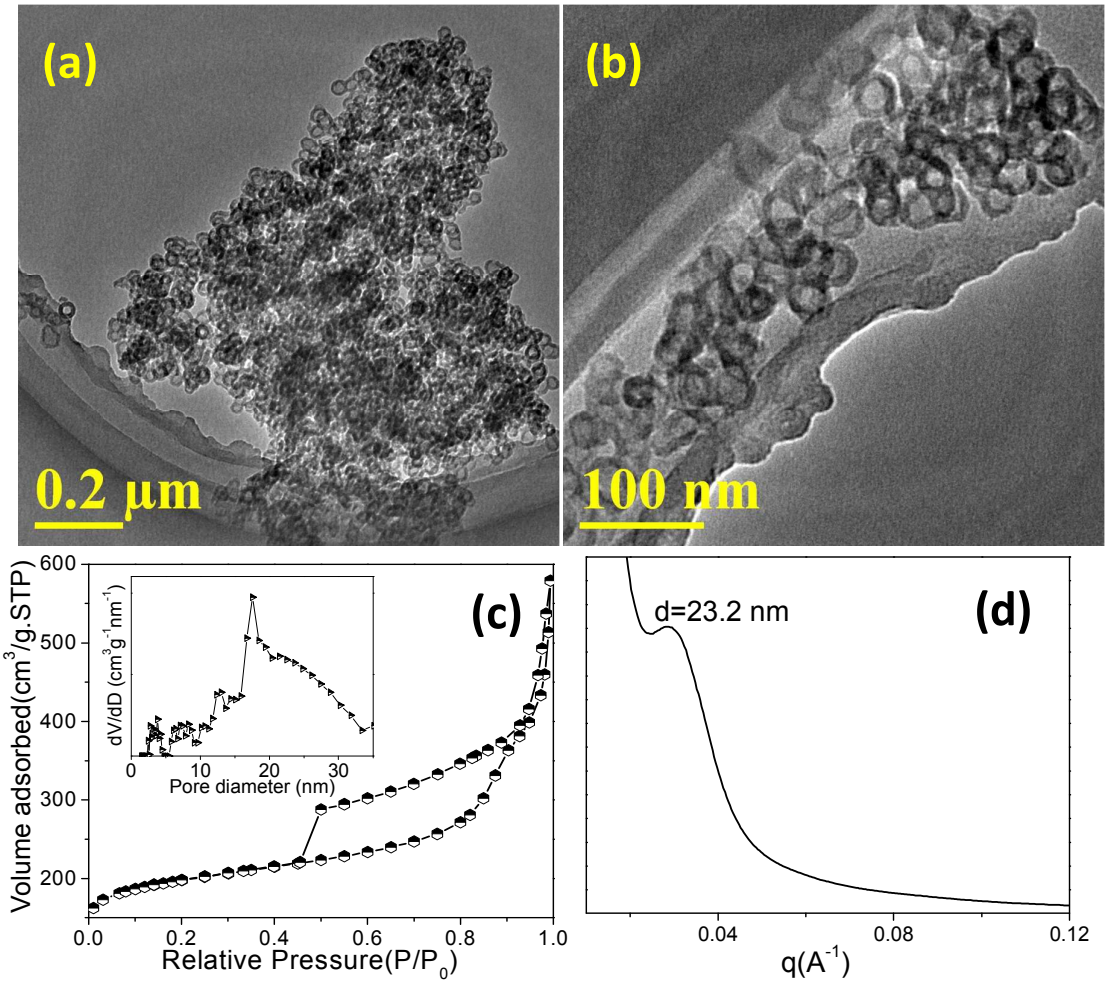

Figure 5. (a, b) TEM images of single hollow carbon spheres (HCSs), (c) nitrogen adsorption-desorption isotherm and NLDFT pore diameter distribution curve from adsorption branch (inset of c) of HCSs, (d) SAXS pattern of HCSs.

Nanoscale Accepted Manuscript

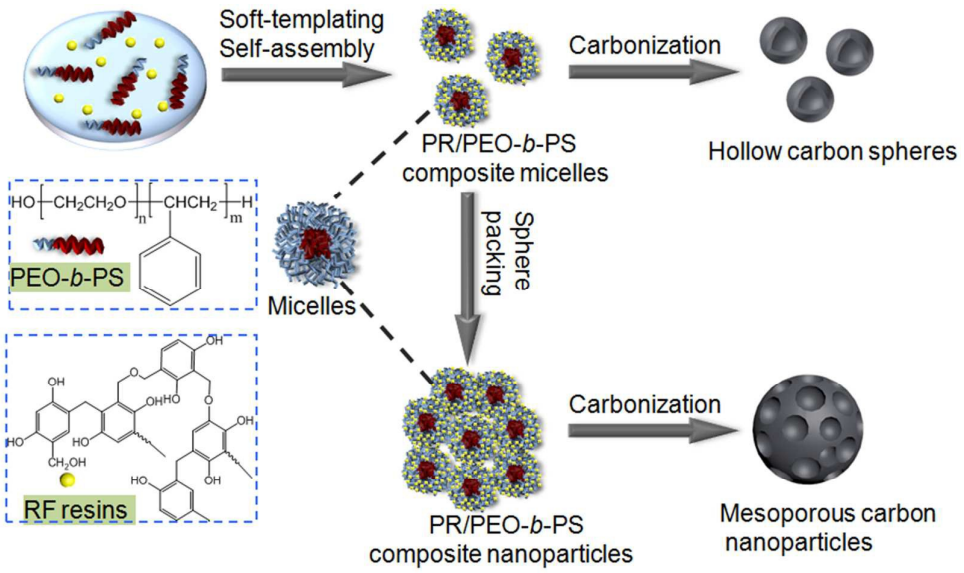

Scheme 1. Schematic illustration of the formation process of the mesoporous carbon nanoparticles (MCNs) by a soft-templating/sphere packing pathway.

Nanoscale Accepted Manuscript

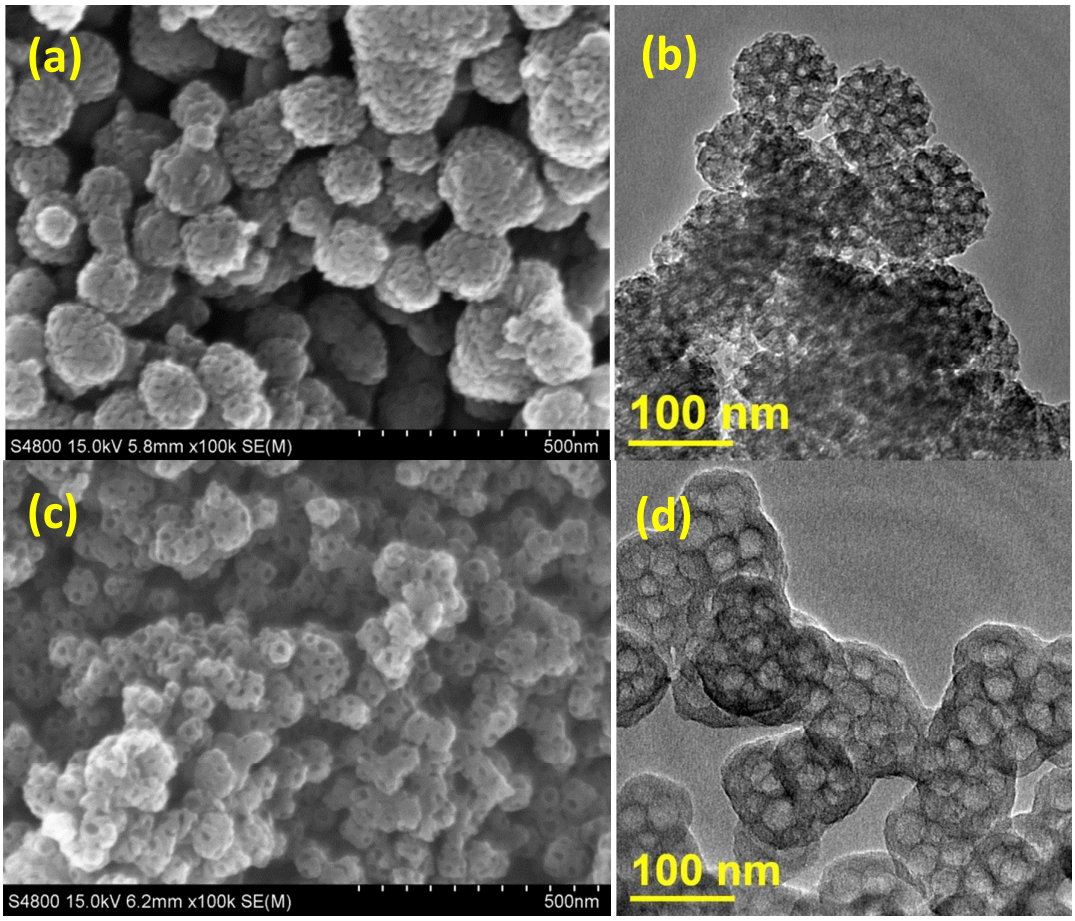

Figure 6. (a, b) SEM image and TEM image of MCN-0, (c, d) SEM image and TEM image of MCN-2.

Nanoscale Accepted Manuscript

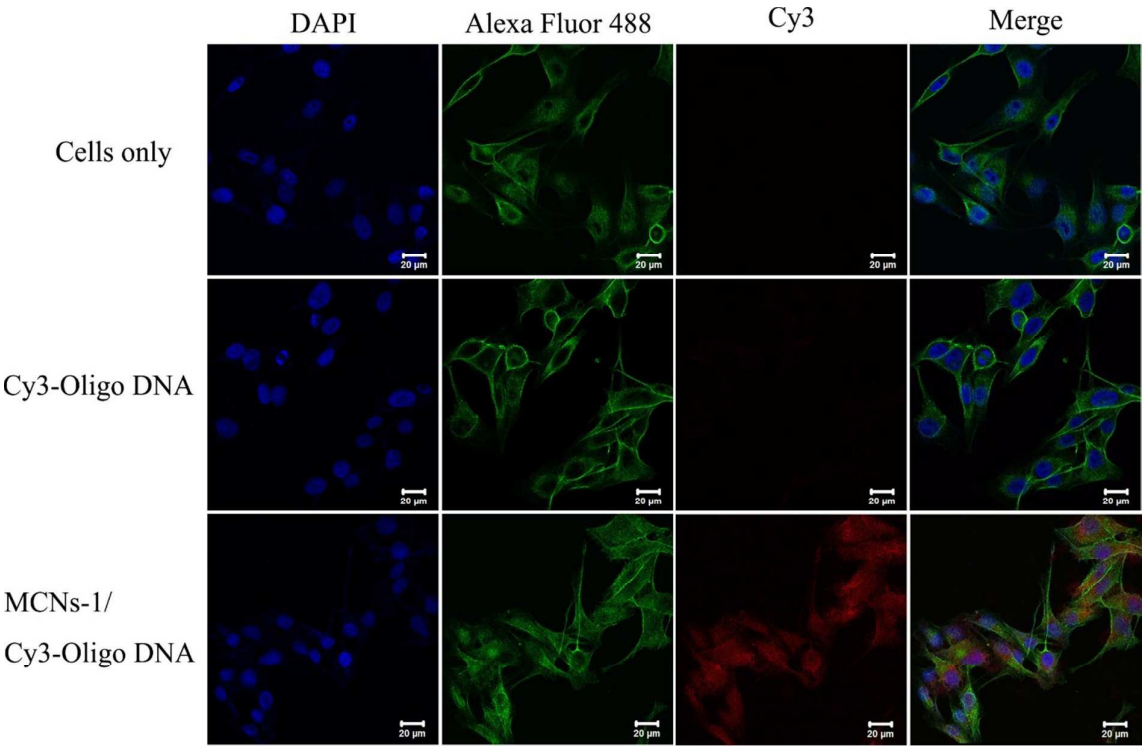

Figure 7. Confocal microscopy images of HCT-116 cells only without any treatment (first row), with the treatment of free Cy3-Oligo DNA (100nM) (second row), the complex of MCNs-1 (80 ug/ml) and Cy3-Oligo DNA (100nM) (third row). The cytosols and nuclei in cells were stained by Alexa Fluor® 488 phalloidin(green) and DAPI (blue), respectively.

Nanoscale Accepted Manuscript